JOURNAL OF GEOPHYSICAL RESEARCH, VOL. 113, D14S19, doi:10.1029/2007JD009106, 2008

Satellite observations of the impact of weak volcanic activity on marine clouds

Santiago Gassó[1]

Received 28 June 2007; revised 24 September 2007; accepted 17 December 2007; published 1 April 2008.

[1] Because emissions from weak volcanic eruptions tend to remain in the low troposphere, they may have a significant radiative impact through the indirect effect on clouds. However, this type of volcanic activity is underreported and its global impact has been assessed only by model simulations constrained with very limited observations. First observations of the impact of high-latitude active volcanoes on marine boundary layer clouds are reported here. These observations were made using a combination of standard derived products and visible images from the MODIS, AMSR-E and GOES detectors. Two distinctive effects are identified. When there is an existing boundary layer cloud deck, an increase in cloud brightness and a decrease in both cloud effective radius and liquid water content were observed immediately downwind of the volcanoes. The visible appearance of these ''volcano tracks'' resembles the effect of man-made ship tracks. When synoptic conditions favor low cloudiness, the volcano plume (or volcano cloud) increases significantly the cloud cover downwind. The volcano cloud can extend for hundreds of kilometers until mixing with background clouds. Unlike violent eruptions, the volcano clouds reported here (the Aleutian Islands in the North Pacific and the South Sandwich Islands in the South Atlantic) have retrieved microphysical properties similar to those observed in ship tracks. However, when comparing the volcano clouds from these two regions, liquid water content can decrease, increase or remain unchanged with respect to nearby unperturbed clouds. These differences suggest that composition at the source, type of eruption and meteorological conditions influence the evolution of the cloud.

Citation: Gassó, S. (2008), Satellite observations of the impact of weak volcanic activity on marine clouds, *J. Geophys. Res.*, *113*, D14S19, doi:10.1029/2007JD009106.

1. Introduction

[2] Although models indicate that natural and anthropogenic aerosols influence cloud formation and cloud properties such as lifetime, precipitation and brightness [*Intergovernmental Panel on Climate Change*, 2001], only in the last 20 years have observations been able to confirm or substantiate some of these effects. For example, there are several examples of observed anomalous cloud brightness and cloud droplet modification in regions dominated by smoke [*Kaufman and Nakajima*, 1993; *Kaufman and Fraser*, 1997] or pollution [*Brenguier et al.*, 2000; *Ramanathan et al.*, 2001a]. Thanks to the relatively recent availability of a new generation satellite detectors [*King et al.*, 1992; *Breon and Goloub*, 1998], spaceborne measurements confirmed that anthropogenic aerosol emissions alter cloud fraction and cloud albedo [*Ramanathan et al.*, 2001b]. Cloud properties such as cloud fraction, cloud effective radius and aerosol properties such as optical depth can be all retrieved simultaneously from the same platform [*King et al.*, 1992]. Thus, it is possible to study cloud optical properties with the coincident presence of aerosols. The measurable effect of aerosol on cloud's albedos is particularly noticeable downwind of major anthropogenic sources such as in ship stacks [*Radke et al.*, 1989]. The detection of precipitation changes due to aerosols [*Albrecht*, 1989] has been more difficult to observe from satellite platforms because the difficulty to collocate satellite precipitation information with cloud and aerosol retrievals. However, there are recent studies have shown the effect of smoke [*Rosenfeld*, 1999; *Andreae et al.*, 2004] and pollution [*Rudich et al.*, 2003; *Rosenfeld*, 2000; *Gavati and Rosenfeld*, 2004] on precipitation. A common feature in these studies is the nature of the aerosol studied; they were all of anthropogenic origin. Notably, there is significant lack of similar observations on clouds (particularly marine clouds) downwind of natural sources such as volcanoes. Marine stratocumulus clouds contribute significantly to the global albedo and are very sensitive to variations in aerosol concentrations [*Twomey*, 1991]. However, there are still important unknowns regarding the factors modulating their origin and precipitation [*Stevens et al.*, 2003; *Wood et al.*, 2002; *Rosenfeld et al.*, 2006]. A good example of the sensitivity of marine clouds to aerosols is provided by the study of ship tracks where it has been observed suppression of rain and increased cloud brightness [*Radke et al.*, 1989; *Coakley et al.*, 1987]. These experiments

[1]Goddard Earth Science and Technology Center, University of Maryland, Baltimore County, Baltimore, Maryland, USA.

0148-0227/08/2007JD009106$09.00

corroborate that marine stratocumulus are very sensitive to changes in aerosol concentrations [*Twomey*, 1991].

[3] Volcanoes are good examples of localized sources with emission of high concentration of aerosols and gases Volcanoes are important because their impact on climate. At timescales of the order of 1 year to a decade, volcanic activity plays a significant role as natural contributor to global climate forcing [*Robock*, 2000]. A number of large-scale eruptions in the last 25 years (e.g., El Chichón, Pinatubo) provided natural experiments where the extent and duration of the climatic response was monitored extensively and used to corroborate model simulations [*Russell et al.*, 1993; *Robock*, 2000]. Most of the studies on the climate impacts of volcanoes have focused on eruptions that inject large quantities of tephra (volcanic ash) into the high troposphere and stratosphere where the residence time is of the order of months to years thus with a potential of a long-term climate impact. Approximately 25% of volcanic eruptions are explosive and they reach the stratosphere. It is estimated they contribute to 60% of the total volcanic SO_2 emitted to atmosphere [*Halmer et al.*, 2002]. Emissions into the troposphere are contributed by nonexplosive eruptions and permanent quiescent volcanoes [*Stoiber et al.*, 1987; *Halmer et al.*, 2002; *Mather et al.*, 2003]. The tropospheric contribution is a significant component to the total natural SO_2 burden [*Andres and Kasgnoc*, 1998] and it has been pointed out that these emissions can have a climatic impact at least as important as the anthropogenic SO_2 emissions [*Graf et al.*, 1998]. The different residence times, the height of emission and the proximity to clouds are all conditions that favor the aerosol direct and indirect effects at local and regional scales [*Graf et al.*, 1997]. There are very few reports of observed effects of volcanic emissions on tropospheric clouds and it is unknown the extent of such interactions. One such study was done by *Tupper et al.* [2005] who analyzed a handful of cases involving convective cumuli clouds during the Pinatubo eruption and confirmed the impact of low-level emissions in several properties such as radar reflectivity and cloud top temperature. However, studies of the mechanisms and the effects of low-level volcanic emissions on marine stratocumulus clouds as well as observations of such phenomena are lacking.

[4] Not only volcanic activity is an agent of climate change via its radiative impacts. In addition, volcanic particulate mater can influence marine biological activity [*Sarmiento*, 1993; *Watson*, 1997; *Uematsu et al.*, 2004; *Duggen et al.*, 2007]. In the presence of high concentrations of sulfur dioxide, iron in volcanic aerosol (common in volcanic ashes [*Benitez-Nelson et al.*, 2003; *Duggen et al.*, 2007]), when hosted in a cloud droplet can be turned into a more soluble form and be readily assimilated by marine biomass [*Meskhidze et al.*, 2003]. Thus, an increase of primary productivity can have a significant impact in atmospheric CO_2.

[5] The main objective of this paper is to report observations of the modification of marine boundary layer cloud properties upon the injection of low-altitude volcanic emissions. The examples are drawn from observations made in the region nearby the South Sandwich Islands in the South Atlantic and the Aleutian Islands in the northern Pacific. This analysis is exclusively based on satellite observations and it is descriptive in nature. It highlights the difficulty of studying low-level clouds at high latitudes where the frequent transit of low-pressure centers (with their associated midlevel cloudiness) and the high viewing angles are a serious challenge for a systematic observational study. In addition, it shows how a naturally occurring phenomenon can significantly alter cloud properties. Moreover, these case studies provide useful benchmarks and constraints for modeling the impact of the volcanic emissions on marine boundary layer clouds.

2. South Atlantic Volcanoes

[6] The South Sandwich Islands are located between 56°S and 60°S and 25°W and 30°W and they are located 2000 km southeast of the Malvinas (Falkland) Islands (Figure 1). They consist of a set of 11 named islands arranged in an arch from north to south and they are part of the east edge of the South American plateau subducting beneath the Antarctic plateau. As show in Figure 1a, this is one of the cloudiest areas of the world with the percentage of cloudy pixels (or cloud fraction) well above 90% throughout the year. The islands are uninhabited with the closest human settlement located on South Georgia Island about 250 km northwest of the northern-most island. The islands are snow covered almost year round and are surrounded by sea ice during most of the winter and spring months. All the islands are small, with areas ranging from 0.4 km^2 (Leskov) to 110 km^2 (Montagu) and they all have degassing volcanoes with different degrees of activity (*Patrick et al.*, 2005). The extent and chronology of volcanic activity has not been assessed because of the difficulty in monitoring the area. The Sandwich Islands are situated in the "Roaring Forties" and are subjected to a succession of midlatitude depressions, frontal systems and migratory anticyclones [*Sinclair*, 1994]. The frequent change in synoptic conditions creates difficult conditions for satellite monitoring, in particular the monitoring of low-level emissions that tend to be obscured by midlevel cloudiness. Occasional research expeditions have reported observations of tephra (volcanic debris) deposits and vapor emissions in some of the islands as early as 1820 [*Holdgate and Baker*, 1979]. More recently dedicated remote sensing studies have shown that the two largest islands (Saunders 57.80°S, 26.46°W and Montagu 58.42°S, 26.38°W) have been active several times during the mid-1990s [*Lachlan-Cope et al.*, 2001] and early 2000s [*Patrick et al.*, 2005]. Recent expeditions to the area sponsored by the British Antarctic Survey (BAS) and the South African Weather Service have confirmed that both Saunders and Montagu are still active [*Smithsonian Institution*, 2006]. Especially Montagu has been in eruption for the last four and half years mainly with minor ash explosivity and there have been some large lava effusions since September 2005 (J. Smellie, BAS, personal communication, 2006). Almost real-time automatic detection of global volcanic activity is monitored by the MODVOLC algorithm, part of the HIGP MODIS Thermal Alert System Automatic (http://hotspot.higp.hawaii.edu/). It uses the infrared channels of the MODIS detector on board the satellites Terra and Aqua (four passes per day) [*Wright et al.*, 2004]. Although the technique is more effective in clear skies conditions (a very rare situation

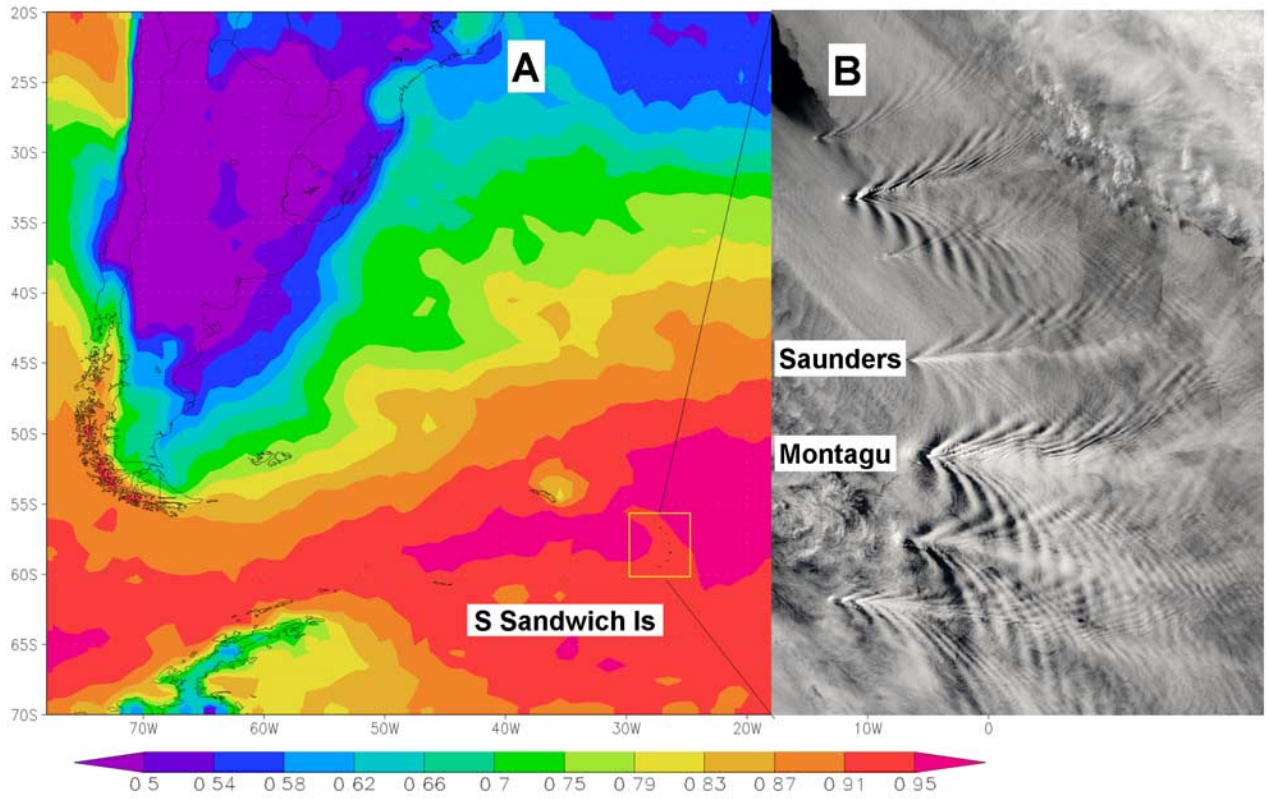

Figure 1. (a) General location of the South Sandwich Islands within a map of the annual average cloud fraction distribution (Terra satellite, figure generated with NASA's Giovanni web interface). (b) Zoom in the area with the two most active volcanoes labeled.

in the area of interest), Montagu and Saunders have shown a detectable infrared signals throughout 2005 [*Smithsonian Institution*, 2005]. In summary, remote sensing of the islands and their volcanic activity is limited because of the synoptic conditions of the area.

[7] Figure 1b is a visible image of the islands and surrounding clouds. Lee waves are visible in each island and they illustrate the fairly high wind speeds prevalent in the area. Midlevel clouds are ubiquitous as it is clear in the upper right and lower left corner of the picture. Note the enhanced brightening in the axis of the wake of the four bottom islands. Although 3-D turbulence effects can result in this brightening (S. Eckermann, Naval Research Laboratory, personal communication, 2006), it is possible that the volcanic emissions are contributing to the observed brightening.

3. Data

[8] This analysis shows data from retrievals made by two satellite detectors. The cloud products from the MODIS detector on board the Terra and Aqua satellites [*King et al.*, 2003] were used to characterize cloud optical properties, cloud top height and temperature and cloud phase. The level 2 (version or collection 005) at 1 and 5 km spatial resolution for both satellites were used. In addition, MODIS visible quicklooks images (500 and 250 m resolution, available from the MODIS Rapid Response System, http://rapidfire.sci.gsfc.nasa.gov/) were used for scene identification, visual description of volcanic activity and checking features not resolved by the Level 2 products. The reader is referred to *Platnick et al.* [2003] and *King et al.* [2003] for more thorough descriptions of the parameters although some of their features relevant to this study are emphasized here. The cloud effective radius (r_{eff}) is a measure of the columnar average droplet size at the top of the cloud. Several studies have shown that CER is a useful parameter to describe the microphysical changes in the cloud droplet distribution upon the injection of aerosols [*Platnick et al.*, 2000; *Schreier et al.*, 2006; *Lin et al.*, 2006]. There is complementary information from the cloud optical depth are (τ), a parameter sensitive to changes in the total droplet number concentration. Under the assumption of vertically homogenous cloud, total amount of liquid water mass is proportional to the product of τ and r_{eff} [*Stephens*, 1978]. This parameter is derived by the MODIS cloud algorithm and reported as liquid water path (LWP). The assumption of cloud vertical structure is particularly relevant in the case of analyzing Level 2 data. Level 2 data is derived from cloud snapshots as opposed to a composite of observations averaged over time and space as is the case of Level 3 data. For example, in situ observations of vertical marine cloud structure show that cloud are not vertically homogenous and often they have an adiabatic or subadiabatic distribution of liquid water content. However, when averaged over time and distance (as is the case in Level 3 data) the vertical structure can be fitted with an adabiatic water profile [*Hobbs and Rangno*, 1998; *Miles et al.*, 2000; *Hegg et al.*, 2007]. Then a particular Level 2 snapshot may or may

not capture clouds that fulfils the vertical homogeneity assumption. As a result, it is useful to consider an independent estimation of LWP. Such additional cloud information can be obtained from the passive microwave AMSR-E detector. As it is on board Aqua, it makes collocated measurements in space and time with MODIS cloud observations. Liquid water path retrievals made by the AMSR-E microwave radiometer are based on a different approach than the MODIS method. Because cloud droplets behave as Rayleigh absorbing particles at the low frequencies of AMSR-E, the mass of the droplets is directly proportional to its emissivity and so is the optical depth of the water cloud in the microwave regime [*Wentz*, 1997]. This is a more direct measurement of total water mass in the cloud than MODIS. Another parameter available (and used in this analysis) from the same retrieval scheme of AMSR-E is the sea surface temperature (SST). Unlike visible and infrared radiances measured by MODIS, microwaves can penetrate clouds and the measured radiances by AMSR-E contain information of the surface emissivity which can be related to surface temperatures [*Wentz and Meissner*, 2000]. The data used were the Level 2 (version 5) daily data gridded at 0.25° resolution and processed by Remote Sensing Systems (http://www.ssmi.com/) following the *Wentz and Meissner* [2000] algorithm. Studies of collocated MODIS and AMSR-E LWP demonstrate that both retrievals agree very well in completely cloudy scenes. AMSR-E LWP retrievals do not distinguish between clear and cloudy skies within the pixel and it is in these conditions were the discrepancies between both detectors are significant [*Horváth and Davies*, 2007; *Bennartz*, 2007].

4. Observations

[9] The case studies were found by browsing high-resolution MODIS visible pictures for the time period March–August 2006. The selection of this time period is based on the fact that the volcanoes were particularly active and as a result, a high likelihood of finding cases of volcanic emissions influencing clouds. Approximately 28 cases were selected with a clear view of volcanic plumes and anomalous cloud brightness in the low-level clouds downwind. These cases were further screened for the availability and quality of microphysical properties retrieved by MODIS. Because at this time of the year (austral fall and winter), low solar zenith angles were frequent, the retrieval algorithm screened out those pixels with low zenith angles and no retrievals were performed in many cases. Even when a retrieval was successful, it must be recognized that these viewing angle conditions are not ideal for cloud retrievals, for example low sun zenith angles and inhomogeneous clouds [*Varnai and Marshak*, 2007] and partially filled pixels [*Coakley et al.*, 2005] bias the retrievals. Although MODIS cloud retrievals are sensitive to 3-D effects such as shadowing [*Marshak et al.*, 2006], it should not be significant in shallow clouds like the ones analyzed here [*Vant-Hull et al.*, 2007; *Segrin et al.*, 2007].

[10] With respect to microwave retrievals, the limitations are of a different nature. The lower ground resolution and the lack of discrimination of cloudy or clear sky within the pixel of AMSR-E make comparison with MODIS data difficult [*Horváth and Davies*, 2007; *Bennartz*, 2007]. Also, the presence of sea ice around the islands (very common during the austral winter) biases the retrievals of SSTs and LWP. In order to characterize boundary layer clouds, cases with midlevel cirrus or stratus and sea ice (as seen in MODIS visible and near-IR images) were avoided. After screening for all these conditions, only a few examples were found among images with visible volcano effects on clouds and simultaneous successful cloud retrievals from more than one detector on the same day. Among those, the following examples are extracted to illustrate the effect of volcanic emissions on clouds.

4.1. Impact of Liquid Water Content

4.1.1. Description

[11] Figure 2a is a visible image from MODIS-Aqua (granule or pass 1615 UTC, 27 April 2006) of the South Sandwich Island region with enhancement in the coloring to better emphasize the cloud contrast. The air mass in the area was influenced by a high-pressure center located approximately at 56°S, 20°W. A fairly homogenous cloud deck of stratocumulus surrounded the islands. Figure 2a shows a clear enhanced brightening in the clouds downwind of the volcanoes. This feature is referred as ''volcano track'' throughout the rest of the paper. Two overlapped volcano tracks are identified. The furthest north track originates in Mount Saint Michael (990 m asl) in Saunders Island and located 60 km south, the second track originates in Mount Belinda (1370 m asl) in Montagu Island. Downwind, increasing midlevel stratus and cirrus obstruct the whole extent of the volcano track. However, the visible image makes apparent the long extent of the volcano track with a minimum length of 400 km. The width of the volcano track (~35 km) is of the order of several level 2 MODIS pixels and it contrasts remarkably in size with ship tracks which tend to be narrower. The water phase at the top of these clouds was detected by the MODIS cloud algorithm (parameter labeled Cloud_Phase_Infrared) as liquid clouds.

4.1.2. Volcano Track Height

[12] The height of the volcanic plume with respect to cloud's height is critical to determine whether this phenomenon is similar to ship tracks. Unfortunately, a direct measurement of cloud deck height is not available for the cases shown here. In fact, the CALIPSO satellite with a lidar on board was launched on 28 April 2006 (same day of one of the observations reported here) and did not start to produce science data until a few months later. However, cloud top parameters and high-resolution (250 m) visible images from MODIS provide useful information. By zooming in on the visible images, it is clear that both Saunders and Montagu islands are cloud covered and no plume above cloud is obvious. This indicates that the top of cloud height is at least as high as Montagu's top (1.4 km). Although the cloud top heights product of MODIS are available for this case, it has been pointed out recently that the MODIS algorithm retrieves cloud height with a very large error [*Naud et al.*, 2005]. However, the spatial variability of the brightness temperatures at 11 μm (a band used in the cloud height retrieval because its emittance is directly related to the cloud top temperature) can provide useful information. They show a gradient from north to south in brightness temperatures. More importantly, there is no difference in temperatures between clouds inside the volcano track and those

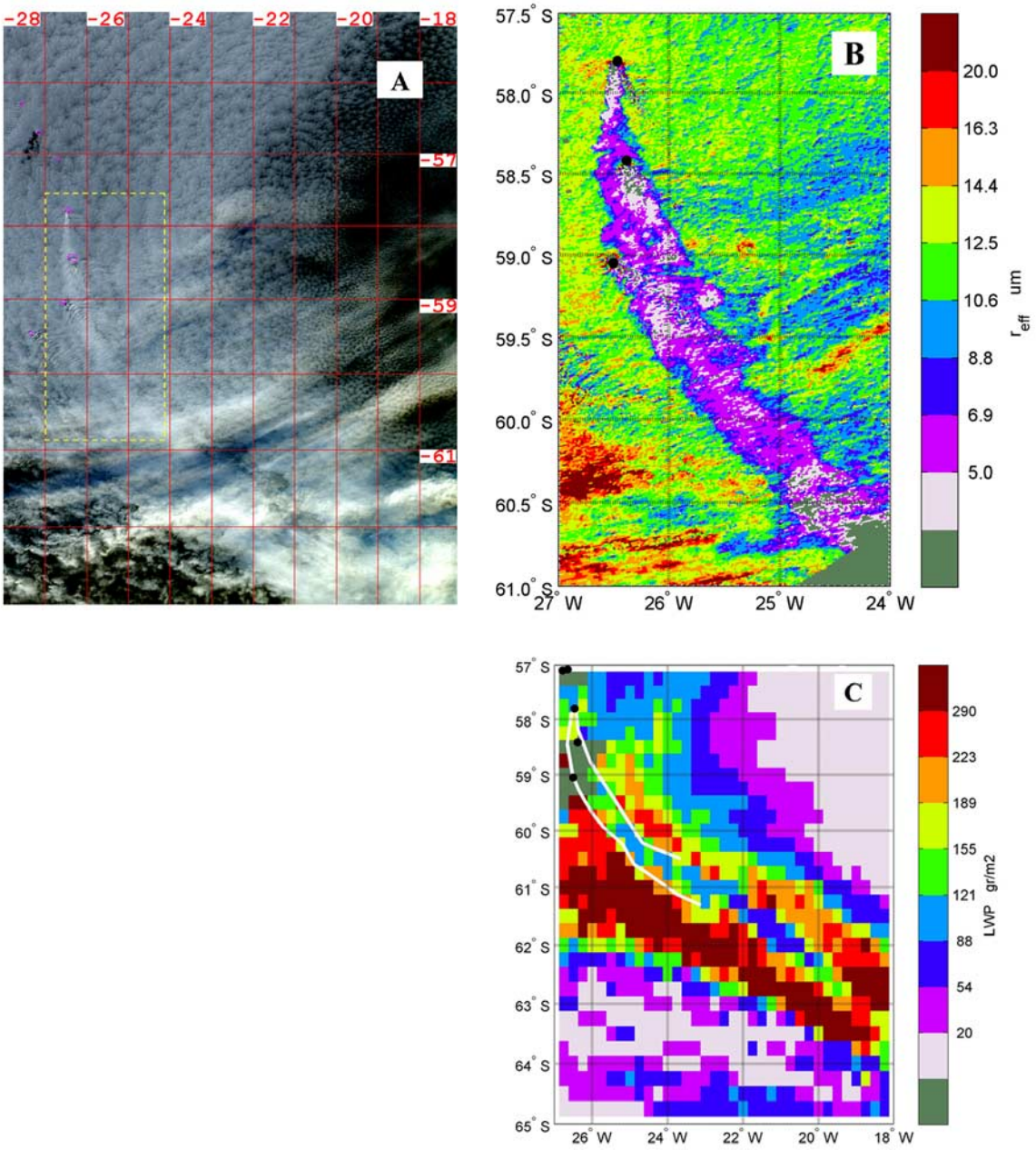

Figure 2. (a) Visible image of the South Sandwich area from MODIS-Aqua for 27 April 2006 (1615 UTC). (b) Cloud effective radii (r_{eff}) retrieved by MODIS-Aqua for the box shown in Figure 2a. (c) A regional view of the distribution of cloud water path retrieved by AMSR-E on board the Aqua satellite. The white line is the envelope of 10 μm r_{eff} from Figure 2b.

pixels immediately surrounding the track; that is, there is no gradient in temperature in the direction perpendicular to the track. Then, the fact that neither the islands nor a volcano plume above cloud are visible and there is no brightness temperature difference between the volcano track and the surrounding clouds, suggest a weakly buoyant volcanic plume at or below cloud level.

4.1.3. Cloud Microphysical Properties

[13] Figure 2b shows the r_{eff} corresponding to the box drawn in Figure 2a. The volcano track is very distinctive compared to the surrounding unperturbed clouds. The r_{eff} threshold between volcano track and background clouds is approximately 11 μm. Inspection within the volcano track reveals variability of r_{eff} suggesting some internal structure with a tendency to have smaller values toward the central axis. For example, south of 59.5°S and starting from the edges, the r_{eff} decrease from the range 8.8–10.6 μm (blue) to the range 6.9–8.8 μm (dark blue) to smaller radii (less than 6.8 um, light and dark pinks). The largest concentration of pixels with very small r_{eff} tends to be immediately downwind of both volcanoes although there are pockets of similarly small r_{eff} further downwind. Mixing in the track is apparent in its east side as indicated by the larger lobes of large r_{eff} intruding. Regarding the droplet size changes

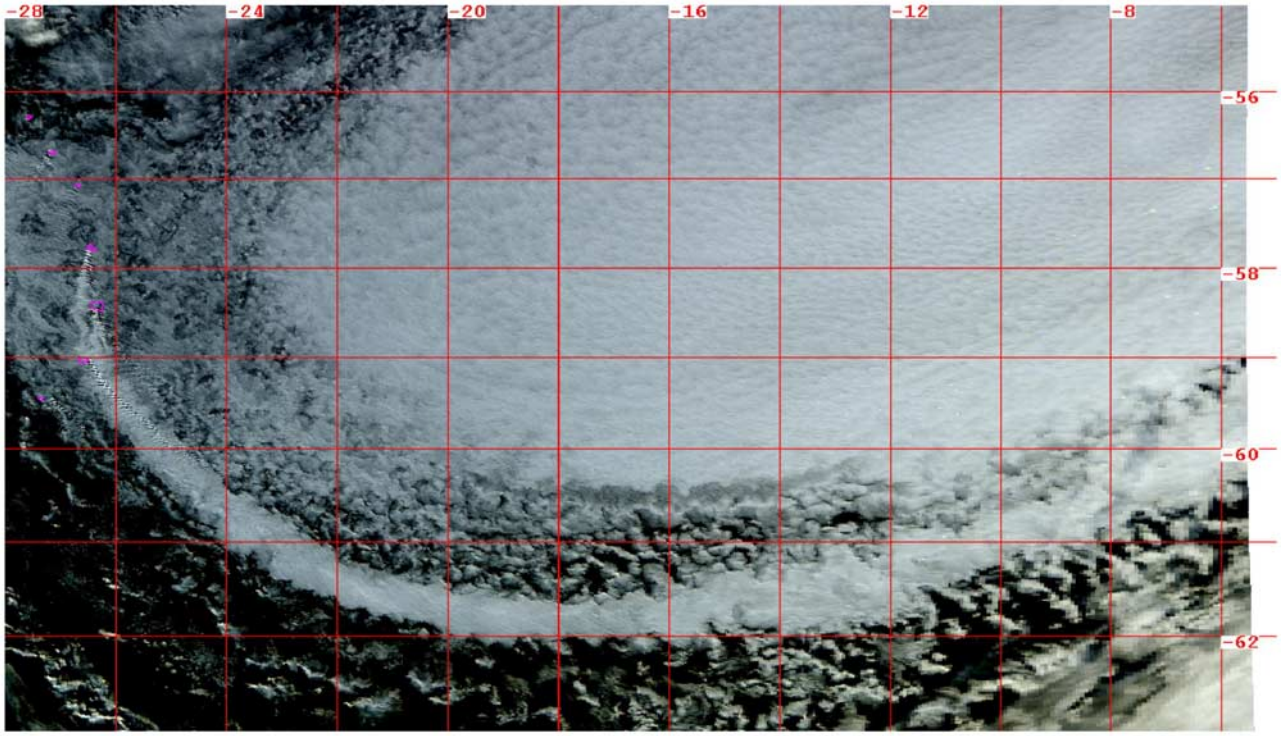

Figure 3. Visible image from MODIS-Terra for 28 April 2006, 1120 UTC. The volcano cloud originating in Montagu and Saunders islands (marked by two pink dots) is visible in the top left and bottom margins.

along the track, there is no significant trend in increasing or decreasing r_{eff}. Figure 2c shows the LWP retrieved by AMSR-E simultaneously with MODIS retrievals. The displayed area matches approximately the area displayed in Figure 2a and the envelope of the 10.6 μm effective radius is included. There is a clear decrease in LWP within the volcano track when compared with the immediately surrounding clouds. Also, the volcano track appears to extend further downwind than what Figure 2a suggests. If assuming an arbitrary threshold of 0.12 kg/m^2 for the distance between the south edge of the envelope to the transition to background (blue to green in Figure 2c, around 62.1°S, 20°W), then the volcano track detected by AMSR (and not seen by MODIS) is approximately 220 km. Thus the total minimum length of the volcano track is of the order of 640 km. In the box outlined in Figure 2a where MODIS and AMSR-E retrievals overlap, there is a contrast between background clouds and the volcano track and there is a minimal intrusion of midlevel clouds. Because of this overlap, it is possible to determine whether intermediate (or midlevel) clouds are present and decide whether the AMSR-E LWP is representative of the low-level clouds only or a combination of low-level and midlevel clouds. For example, south of 60.5°S, the MODIS visible image (Figure 2a) shows midlevel clouds advecting into the field of view of AMSR-E and the cloudiness increases further to the south totally obstructing the volcano track. Then, the AMSR-E LWP retrievals south of the envelope are representative of the both low-level and midlevel clouds. However, the pattern of change in the water path in this region is coincident with the continuation of the volcano track and not with the pattern of midlevel clouds (which move in from west to east).

[14] A decrease or near constant in liquid water content in marine stratocumulus has been observed previously in ship tracks using remote sensing [*Platnick et al.*, 2000; *Coakley and Walsh*, 2002; *Matsui et al.*, 2006; *Segrin et al.*, 2007] and reported by in situ studies [*Ferek et al.*, 1998; *Twohy et al.*, 2005]. An explanation to the reduction of cloud water content was offered by *Ackerman et al.* [2004] and *Guo et al.* [2006] who suggested that the presence of small droplets enhances the entrainment of dry air from aloft resulting in precipitation suppression effect. In this case, no information of precipitation is available and the humidity levels above the cloud deck are unknown. However, the presence of a high-pressure center NE of the volcanoes (clear sky area in Figure 2a) suggests the presence of subsiding dry air above the clouds.

4.2. Modification of Cloud Fraction

4.2.1. Description

[15] The effect of modification of cloud fraction is illustrated with a case observed the day after. Although the high-pressure center located NE of the islands shifted to the E, the synoptic conditions were similar to the previous day. The Saunders and Belinda volcanoes and their impact on clouds continued throughout the night since the AMSR-E nighttime pass (0200 UTC, not shown) measured a depression in LWP immediately downwind similar to Figure 2c. Figure 3 is a visible picture taken by MODIS-Terra (1120 UTC pass). The effect of the volcanic emissions in the broken cloud field is clearly visible in the bottom half

of Figure 3. South of the cloud deck, a continuous and compact cloud (referred to here as "volcano cloud") with origin in the Michael and Belinda volcanoes is apparent. The length is approximately 1300 km from Saunders to the edge of the picture and it may extend further east. The width of the volcanic cloud triples from its beginning to its end (40 km wide at 26.40°W, 50 km at 20.35°W, 78 km at 14.35°W and 140 km at 5.7°W). The disruption in cloud fraction due to the volcanic cloud is very clear in an area where there would otherwise have just been dissipating open cells. In addition, the cloud deck and clouds surrounding the volcanoes are in liquid phase according to the MODIS cloud products. Like the day before, the background conditions are still determined by the presence of a high-pressure system with the center located near the upper right corner of Figure 3. Reanalysis data from the Global Data Assimilation System (GDAS [*Derber et al.*, 1991]) surface pressure shows a decrease poleward and coincides with the gradual decrease in cloud fraction from north to south.

[16] Inspection of high-resolution visible pictures (250 m) reveals a very white cloud in a v shape with vertex in both volcanoes and superposed with orographic clouds originating in each volcano. It should be pointed out that the white color of the cloud is a qualitative indicator of a plume rich in liquid or iced droplets (with a resulting flat spectral dependence in the visible) as opposed to a plume rich in ashes and aerosols which has a yellowish or brownish color in the visible images. Wind conditions favored the merging of Michael's cloud with the Belinda's cloud forming a single long volcano cloud. In addition, wave patterns consistent with lee waves are visible in both clouds. Also, the lee waves are visible in a (nonactive) volcanic island south of Montagu (Bristol Island) and these waves reach the volcano cloud. The image shows cloud banding consistent with a purely diverging mountain wave pattern or "shiP waves" [*Sharman and Wurtele*, 1983; *Eckerman et al.*, 2006] although only the north arm of this v-shaped pattern is fully visible, the south arm is still being partially dampened possibly because of variations in wind shear. The superposition of lee waves on top of the volcano cloud disappears approximately 100–150 km downwind. Northeast and east of the islands, a large deck of stratocumulus clouds shows a pattern of transition from closed cells to open cells toward its south edge. This behavior is typical in evolving marine stratocumulus [*Stevens et al.*, 2005; *Rosenfeld et al.*, 2006] where cloud droplets reach a critical size, start to fall removing aerosols from the column and leaving behind a clean and clear area (or open cell). From the viewpoint of satellite retrievals, closed cell clouds have relatively small cloud effective radius ($r_{eff} \sim< 15$ um) and large liquid water path (LWP $\sim> 0.3$ kg/m^2) whereas open cell clouds have larger and smaller r_{eff} and LWP respectively.

4.2.2. Cloud Microphysical Properties

[17] The effective radii are shown in Figure 4a with the compact cloud deck with low values in the upper right transitioning to larger values and decreased cloudiness in the bottom half. It should be noted that some of the retrievals in open cells smaller than 1 km (pixel size used in the retrieval) may be biased because of the total cloudy pixel assumption used in the cloud retrieval algorithm [*Coakley et al.*, 2005; *Marshak et al.*, 2006]. This consideration is particularly relevant to the partially cloudy swath between the volcano cloud and the solid cloud deck to the north. Thus a quantitative comparison of the magnitude of r_{eff} with the immediate nondisturbed clouds may not be correct. However, it is interesting to compare with the more compact cloud deck further north of the volcanic cloud. Also, the values of r_{eff} below 15 μm within the volcano cloud are consistent with other observations in the marine environment of nonprecipitating polluted and nonpolluted marine stratocumulus [*Rosenfeld et al.*, 2006; *Schreier et al.*, 2006; *Segrin et al.*, 2007]. Within the volcanic cloud, there is longitudinal and transversal variability indicating a highly dynamic system. For example, there is a gradual transition in r_{eff} from W to E. Beginning near 18°W, r_{eff} starts to increase and it has comparable values to those of the cloud deck to the north, then by 12°W the volcano cloud signature starts to become more like the surrounding clouds and by 6°W it is almost undistinguishable. In its first half, there is little symmetry of r_{eff}s with respect to the longitudinal axis and smaller r_{eff}s (blues) are more predominant in the northern edge. The second half of the volcano cloud shows a more symmetric distribution of r_{eff}s with respect to the major axes. Cloud optical depths and the derived liquid water paths for the same picture reveal additional information (Figures 4b and 4c). High (>40) and homogenous values of τ are prevalent throughout the first half up to 18°W and then they are more variable, with a decreasing tendency toward the tail. Out of the volcano plume, τs are significantly smaller (<10), typical of clean marine clouds. The width of the volcano cloud as determined by the τs is smaller than the width shown in the r_{eff} (Figure 4a). Zooming in the pixels near the edges, the τs smoothly transition toward the background values in contrast to the r_{eff} which have sharp increase at the edges. Also, the shape and visual texture of edges suggests mixing with surrounding air. LWP distribution (Figure 4c) makes more apparent the variability within the volcano cloud noted in the r_{eff}s and τs. For example, LWP is high in the first half of the volcano cloud with smaller values toward the edges. Then after a brief decrease (~18–12°W), the LWP increases toward the end with a variability modulated by the τ (compare Figures 4b and 4c). Although the LWP values within the volcano cloud are higher than the immediately surrounding background clouds, these background clouds are very inhomogeneous and possibly with variable cloud fraction within the 1 km pixel, bringing into question the quality of the retrievals as it was mentioned earlier. However, the magnitude of the LWP in the volcano cloud is similar to the LWP in the homogenous and more compact cloud deck north of it.

4.2.3. Diurnal Variability

[18] Some insights of the evolution of the volcanic cloud can be gained by comparing the retrievals from the Terra pass with the Aqua pass 4 h later (Figures 5a, 5b, and 5c). Because the low solar zenith angle, the algorithm retrieved properties only in the west half of the volcano cloud. The region of small droplets ($r_{eff} < 8.75$ um) within the volcano cloud extended further east and toward the north edge. The presence of lobes (in Figure 5a) on both sides of the cloud giving a meandering look to the r_{eff}s < 8.75 μm suggests mixing processes at play. This is reinforced in the change in cloud optical depths from the morning to the afternoon. In

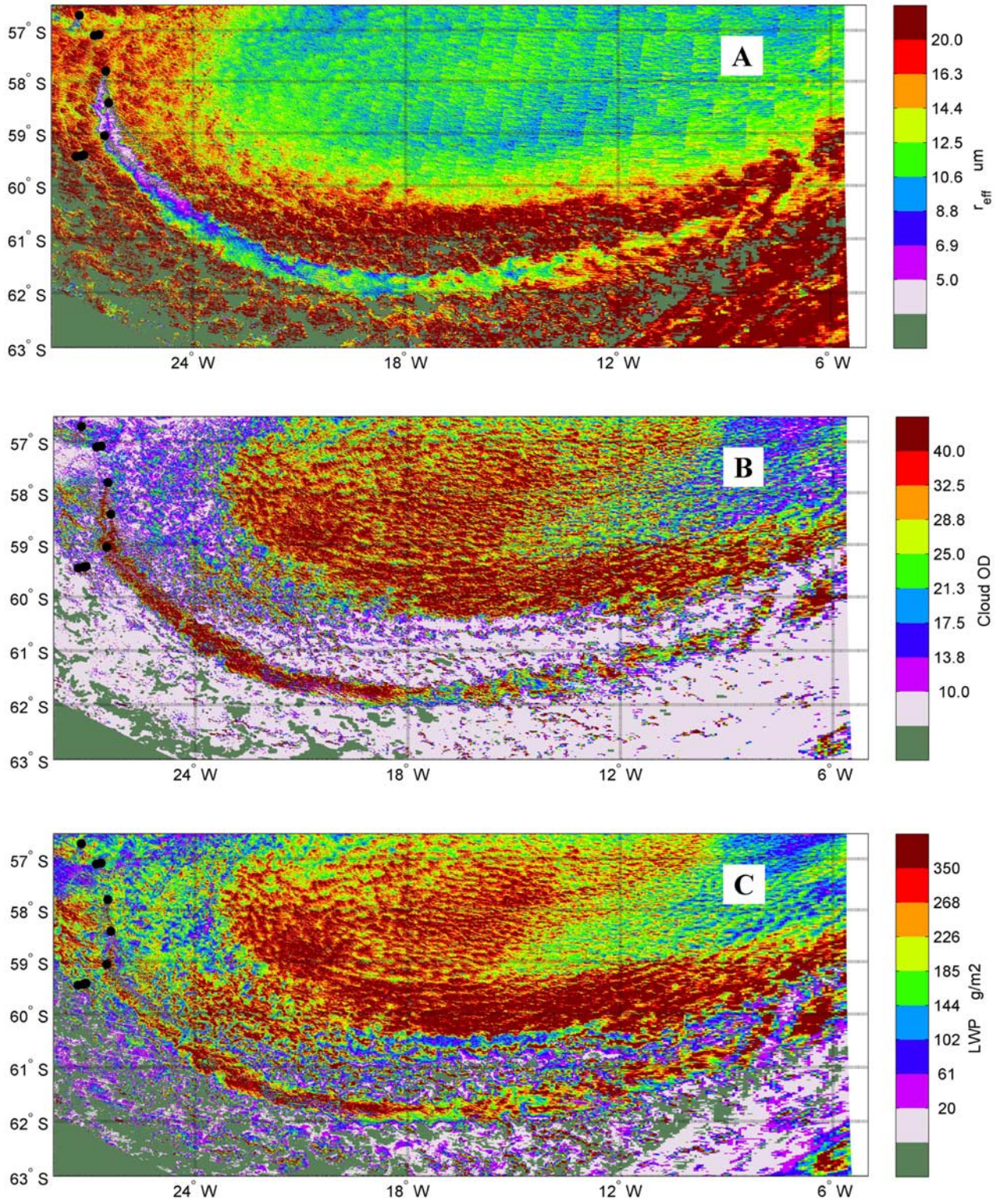

Figure 4. MODIS-Terra retrieved parameters for 28 April 2006 (1120 UTC). (a) Cloud effective radius (r_{eff}, in μm), (b) cloud optical thickness (COT, unitless) and (c) liquid water path (LWP, in kg/m^2).

the morning, high τs are prevalent in the west half of the cloud whereas later, there is a decreasing trend. In particular and in the afternoon pass, τs between 24°W and 17°W tend to be higher along the central axis and decrease by a factor of 2 toward the edges. This is reflected in the distribution of LWP with a clear decrease from the morning to the afternoon. Overall the volcano cloud appeared to have lost liquid water and its droplets decreased in size from the

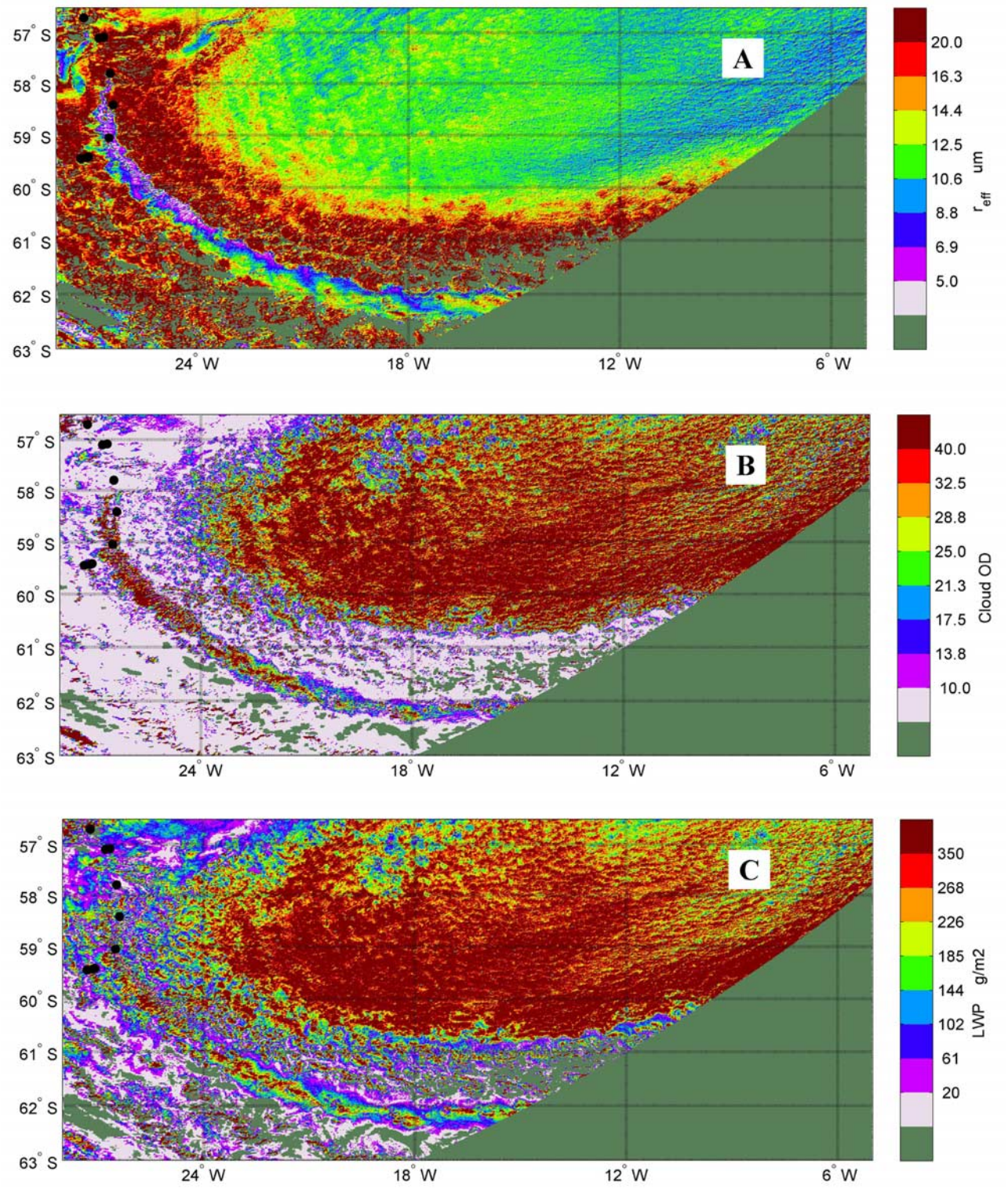

Figure 5. Same day as in Figure 4 but for MODIS-Aqua 1520 UTC.

morning to the afternoon. Diurnal variation of liquid water path is expected at a mesoscale level with maximum in the morning and a decrease throughout the day due to increased solar absorption [*Wood et al.*, 2002]. However, note that the cloud deck north of the volcano cloud appeared to have increased LWP from the morning to the afternoon suggesting that solar forcing is not the only factor modulating the microphysical properties in this case. Another possibility is that the evolution of the cloud is dictated by synoptic conditions. For example, modeled moisture profiles (GDAS) and observed SSTs from AMSR-E (not shown) data show a dry free troposphere aloft and a decreasing flow

of moisture from the surface poleward, all coinciding with the decrease in cloudiness toward the south.

4.2.4. Volcano Cloud Height

[19] Like in the previous day, there are no direct measurements of cloud height available for these observations. However, the brightness temperatures at 11 μm (1 km resolution), high-resolution visible images, cloud top pressure and temperature retrievals (5 km resolution) help to constrain the cloud height. Unlike the case of the previous day, there is no homogenous cloud field immediately next the long volcano cloud. However, there are some clear differences between these height proxies inside and outside the volcano cloud. Brightness temperatures in the volcano cloud are cooler by less than 2 K than the surrounding clouds along the first half of the volcano cloud (up to $\sim$13°W). East of 13°W, the temperature difference reduces gradually until the volcano cloud merges with surrounding clouds. Although the absolute magnitude of the cloud top products of MODIS are not accurate in low clouds [*Naud et al.*, 2005], it is nevertheless worth to point out that they capture a variability consistent with the brightness temperature observations. For example, cloud top pressures in the volcano cloud are slightly smaller with respect to the surrounding clouds. Additionally, the volcano and background cloud tops tend to go up toward the east indicating a possible thickening of the boundary layer. Overall, the volcano cloud is higher than the surrounding clouds. But after 500 km, this difference decreases and volcano cloud and background clouds become indistinguishable as observed by MODIS.

5. Discussion

[20] Because the composition of the volcanic plume is critical in determining the evolution of the resulting volcanic track or cloud, an important consideration is the nature of the volcanic emissions. However, there is limited information on the composition of the volcanic emission that can be inferred from remote sensing platforms. Columnar sulfur dioxide retrievals are available from the OMI detector on board of the satellite Aura but these retrievals are limited to volcanic emissions that reach the free troposphere [*Krotkov et al.*, 2006]. For the cases studied here, the OMI algorithm did not retrieve any columnar SO_2 data. Similarly, the MODIS aerosol algorithm did not retrieve any aerosol optical depth because the lack of clear sky pixels required for such retrievals. However, some information can be inferred on the nature of the volcano cloud and tracks observed. *Prata* [1989] defined a criterion for differentiation between a plume with predominantly liquid water droplets and aerosol precursors and a plume rich in silicates and ashes. The method is based on the differences in emissivity between silicate particles and water and ice particles in the 11 μm and 12 μm channels in AVHRR (equivalent to Channels 31 and 32 in MODIS) identifying positive differences for water clouds and negative for ash containing clouds. The criterion applied to both cases shown here did not differentiate between the volcano influenced clouds and the background undisturbed clouds. This suggests that the volcano cloud on 28 April and the volcano track of 27 April are largely composed of water droplets as opposed to a silicate-rich plume which would have different optical properties in the IR channels of MODIS.

[21] Another important point in the 28 April case is whether the observed volcanic cloud is the result of volcanic emissions inducing cloud formation downwind (such as in the Kilauea volcano in Hawaii [*Cochran and Pyle*, 1978] or in Pinatubo [*Tupper et al.*, 2005]). Alternatively, it is possible that the observed cloud consists of a stationary plume made up of water droplets and gases continually fed by the volcano emissions. Although there are no in situ aerosol measurements available for the South Sandwich Islands volcanoes, it is reasonable to assume that these volcanoes emit large quantities of cloud condensation nuclei as it has been observed in other volcanoes [*Mather et al.*, 2003, 2004]. Thus, whether water droplets form at the emission point depends on the environmental conditions [*Graf et al.*, 1997; *Matsushima and Shinohara*, 2006]. In this case, inspection of high-resolution 250 m images of MODIS a shows white plume originating in each volcano. According to the test defined by *Prata* [1989], this is consistent with a plume rich in liquid water.

[22] Although these observations are based on one region of the globe, the volcano clouds have been observed in other volcanoes such as in the Aleutian Islands in Alaska or in Japan where plumes rich in water droplets and visually behaving like meteorological clouds have been reported (Miyakejima volcano [*Kinoshita*, 1996; *Kinoshita et al.*, 2003]). Figure 6a shows an example of increased cloud fraction downwind of one of the volcanoes located in the Atka Island (52.3°N, 174.1°W), part of the volcanic group in central Aleutian Archipelago [*Siebert and Simkin*, 2002]. Atka contains several occasionally active volcanoes with one known to be frequently active (Korovin, 1553 m). Thermal springs and fumaroles located on and near the volcano indicate an active hydrothermal system as well as occasionally energetic steam emissions of a small lake. Although no report for this specific day is available (4 November 2006), the weekly Alaska Volcanic Observatory (AVO) report raised the aircraft volcanic hazard alert level due to the increase of seismic activity and visual observations of gases and steam coming out the volcano during that week. It should be noted that the AVO does not regularly report weak volcanic activity unless it clearly poses a hazard for aviation (T. Murray, AVO, personal communication, 2006). The GOES 11 satellite band 1 (visible) pictures taken every half hour show a steady low-level cloud that remains for several hours in every picture (Figures 7a–7c span 7 h) despite that environment conditions that favor the break up of clouds as the surroundings clouds indicate. Figure 6 also shows the MODIS retrieved r_{eff} (Figure 6b) and LWP (Figure 6c) and AMSR-E LWP (Figure 6d). An important difference with the observations in the South Sandwich Islands is the lack of marked contrast with respect to surrounding (unperturbed) clouds. For example, effective radii are small immediately downwind the volcano ($r_{eff} < 8.75$ um) and they increase somewhat downwind. However, they are not significantly different from the r_{eff} of the unperturbed cloud deck SW (circa 49.5°N, 178°E) of the volcano cloud. Further, there is no clear sharp transition or edges between volcano and background clouds as was the case shown in Figure 3 (28 April). However, both liquid water path in MODIS and AMSR-E agree in showing an increasing trend within the volcano cloud downwind in contrast with Figure 2 where a decrease was noted. The increase in LWP is

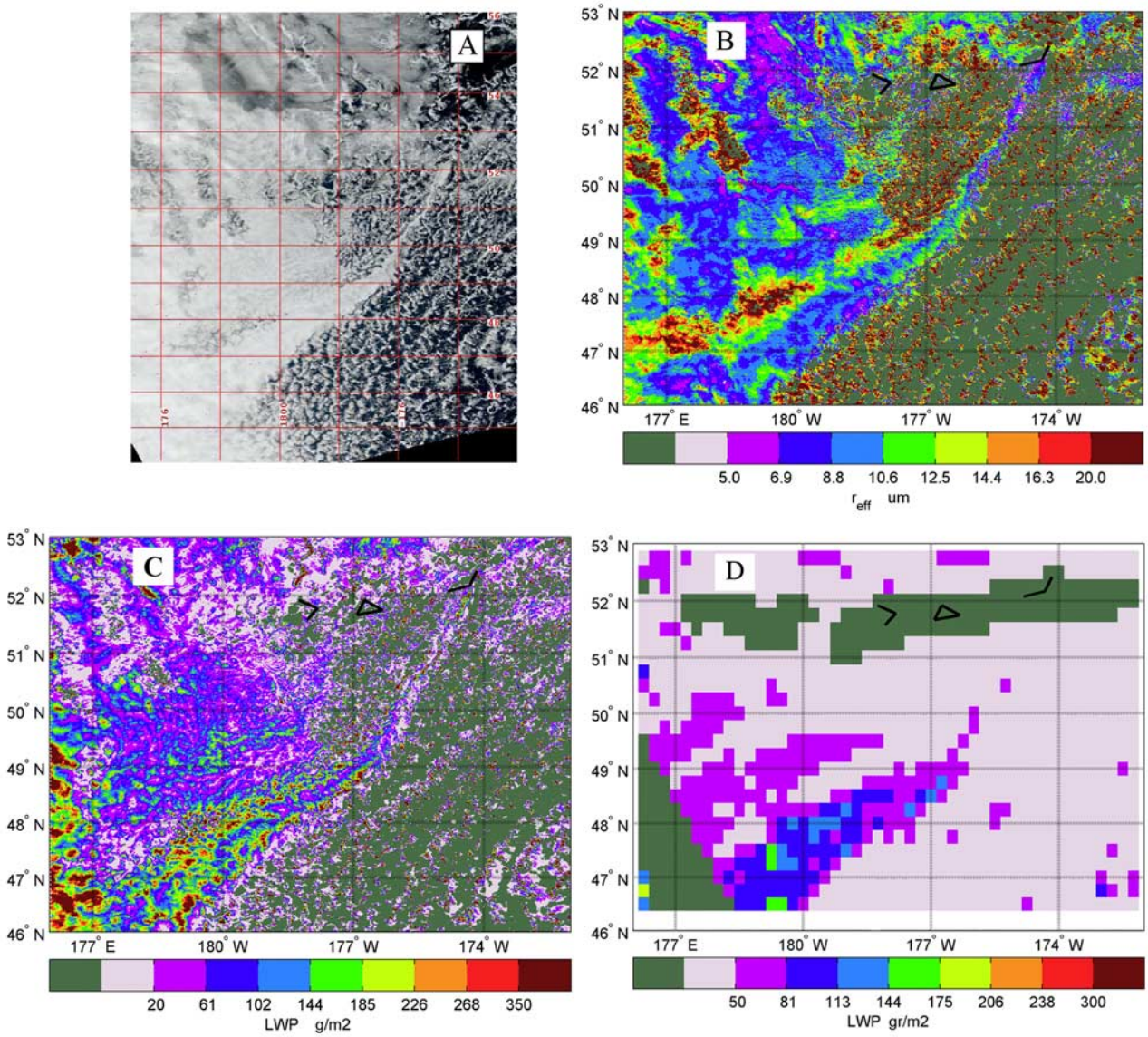

Figure 6. (a) Visible MODIS-Aqua picture taken on 4 November 2006 (0020 UTC) over the Central Aleutians region. (b) MODIS retrieved r_{eff}. (c) MODIS retrieved LWP. (d) AMSR-E retrieved LWP.

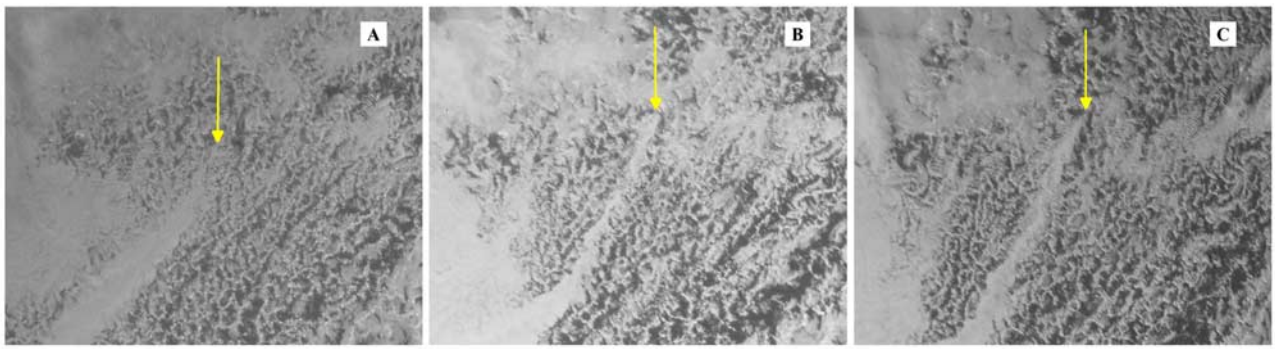

Figure 7. A volcano cloud originating in Atka Island (arrow) is visible in these GOES 11 (band 1) figures on 4 November at (a) 2000 UTC and (b) 2330 UTC and (c) 5 November 0200 UTC. Pictures taken during intermediate times showed the same feature. Photos courtesy of Hawai'i Institute of Geophysics and Planetology GOES site (http://goes.higp.hawaii.edu/).

coincident with a mesoscale increase of SST from north to south as indicated by AMSR-E SST retrievals (not shown). Given the effective radii do not increase significantly; this suggests a possible increase of particle number and/or cloud thickness. Overall, it appears the cloud microphysical features in this case are different than the South Sandwich Islands cases discussed previously. The nature of the volcanic emission probably is critical in determining the microphysical evolution of the volcano plume. The reviews of *Heiken* [1994] and *Mather et al.* [2003] emphasized the wide range components in volcanic ashes and gases that determine how gases condensate onto particles, become cloud condensation nuclei and then to droplet sizes.

[23] The examples here shown highlight the fact that cloud liquid water path can increase or decrease in the presence of high concentrations of aerosol such as those from volcano emissions. Recent modeling studies suggest this behavior is possible and it is very dependent of the background mesoscale conditions. For example, *Ackerman et al.* [2004] and more recently *Guo et al.* [2006] pointed out that despite the high concentration of aerosols in a polluted cloud, a decrease or increase of liquid water content can occur depending on the presence of a dry or humid air mass above the cloud (due to for example, strong or weak subsidence) and whether the cloud is precipitating or not. Although not explored in detailed in this study, it should be pointed out that there is a contrast between the NH and SH cases. For the Aleutian volcano case, the LWP seems to increase with distance while that for the South Sandwich case decreases. The AMSR-E SST data shows that in the NH the plume is propagating toward warmer waters while in the SH it is propagating toward colder waters. This behavior is in agreement with the observations of *Hegg et al.* [2007].

[24] From the three examples, some common features regarding the occurrence of this phenomenon can be pointed out. The fact that the observations reported here occurred at high-latitude volcanoes with summits below 1600 m suggests that emission height as well as boundary layer height should be critical parameters to consider. The phenomena described appear to occur when the volcanic plume is not buoyant enough to break through the temperature inversion and remains in the boundary layer impacting existing clouds. Another possibility is that the weakly ascending plume reaches the level of neutral buoyancy right above the inversion layer and then is quickly dispersed by the high winds in the free troposphere [*Rose et al.*, 1988]. As pointed out by *Kinoshita* [1996], these conditions are usually met by low explosive eruptions and natural gas and vapor emissions. Also, *Self and Walker* [1994] and *Halmer et al.* [2002] emphasize that the permanence of volcanic gases and aerosol at specific height in the atmosphere and impacting clouds depends both on volcanological (chemical composition of magma, strength and duration of eruption, altitude and latitude of volcano) and atmospheric (wind, temperature and humidity profiles). However, as noted by *Graf et al.* [1997], global volcanic networks do not monitor the activity of all volcanoes in the world and it is unknown how many and the frequency of weak eruptions and emission of weak plumes [*Simkin*, 1994]. In the case of the South Sandwich Islands, satellite monitoring based on IR signatures shows volcanic activity in Montagu and Saunders islands since 2001 [*Smithsonian Institution*, 2005]. However, it is uncertain the extent and frequency of the volcanic influence on boundary layer clouds in this region. A non systematic visual inspection of pictures in the historical MODIS database shows numerous examples of volcanic clouds and tracks. For example, several cases were found during the time frame March–August 2006, also cases were found in 2002, 2003 and 2004. In summary, there are indications of frequent instances of volcano clouds and tracks in the South Sandwich Islands. Although in recent years satellites have contributed significantly to global monitoring and observation of volcanic activity, automatic detection schemes do not perform well when clouds are present [*Wright et al.*, 2004] or when emissions of SO_2 remain at low altitudes (<3 km) and at high latitudes with low solar zenith angles [*Krotkov et al.*, 2006], all conditions met by many of the volcanoes in the North Pacific and South Atlantic oceans.

6. Conclusion

[25] The objective of this work is to illustrate that naturally degassing or weakly explosive volcanic eruptions can influence boundary layer clouds significantly by changing their microphysical properties and increase cloud faction. This paper shows first observations of modification of cloud properties due volcanic emissions in the boundary layer. The examples analyzed illustrate a number of features of cloud modification in marine clouds. In comparison with surrounding uncontaminated clouds, a volcano plume influences an existing cloud by decreasing the droplet effective radius, increasing visible brightness and decrease the liquid water path. In addition, it can modify regional cloud fraction by adding cloud cover in an otherwise cloudless area. Like in ship tracks, these observations demonstrate the existence of natural laboratories where studies related to aerosol-cloud studies can be performed. However, these observations highlight some important features not shared with ship tracks. The spatial and temporal scale at which these phenomena occur can be larger than man made ship tracks and given that volcano eruptions are randomly occurring phenomena, it remains to be assessed what role (if any) cloud modification by volcanic emissions in the low troposphere play in climate studies. As noted by the modeling study by *Graf et al.* [1998], the radiative impact can be significant. The observations here reported contribute to the understanding on how volcanoes impact clouds and improve such estimates.

[26] **Acknowledgments.** The author thanks NASA's MODIS Rapid Response system, the Goddard Earth Science Data and Information Services Center (DISC), NASA's Giovanni website and Remote Sensing Systems for making the MODIS and AMSR-E satellite data available and easily accessible. Also, the author wishes to thank Dean Hegg, Nicholas Meskhidze, Steve Platnick, Peter Croot and Eric Wilcox for their useful discussions and suggestions in the preparation of the manuscript. Finally, this work is dedicated to the memory of Yoram Kaufman whose encouragement and enthusiasm when I showed him these findings were the driving force to complete this work.

References

Ackerman, A. S., M. P. Kirkpatrick, D. E. Stevens, and O. B. Toon (2004), The impact of humidity above stratiform clouds on indirect aerosol climate forcing, *Nature*, *432*(7020), 1014–1017.

Albrecht, B. A. (1989), Aerosols, cloud microphysics and fractional cloudiness, *Science*, *245*, 1227–1230.

Andreae, M. O., et al. (2004), Smoking rain clouds over the Amazon, *Science*, *303*(5662), 1337–1342.

Andres, R. J., and A. D. Kasgnoc (1998), A time-averaged inventory of subaerial volcanic sulfur emissions, *J. Geophys. Res.*, *103*, 25,251–25,261.

Benitez-Nelson, C. R., S. M. Vink, J. H. Carrillo, and B. Huebert (2003), Volcanically influenced iron and aluminum cloud water deposition to Hawaii, *Atmos. Environ.*, *37*, 535–544.

Bennartz, R. (2007), Global assessment of marine boundary layer cloud droplet number concentration from satellite, *J. Geophys. Res.*, *112*, D02201, doi:10.1029/2006JD007547.

Brenguier, J. L., P. Y. Chuang, Y. Fouquart, D. W. Johnson, F. Parol, H. Pawlowska, J. Pelon, L. Schuller, F. Schroder, and J. Snider (2000), An overview of the ACE-2 CLOUDYCOLUMN closure experiment, *Tellus, Ser. B*, *52*(2), 815–827.

Breon, F. M., and P. Goloub (1998), Cloud droplet effective radius from spaceborne polarization measurements, *Geophys. Res. Lett.*, *25*(11), 1879–1882.

Coakley, J. A., and C. D. Walsh (2002), Limits to the aerosol indirect radiative effect derived from observations of ship tracks, *J. Atmos. Sci.*, *59*(3), 668–680.

Coakley, J. A., R. L. Bernstein, and P. A. Durkee (1987), Effect of ship-stack effluents on cloud reflectivity, *Science*, *237*, 1020–1022.

Coakley, J. A., Jr., M. A. Friedman, and W. R. Tahnk (2005), Retrieval of cloud properties for partly cloudy imager pixels, *J. Atmos. Oceanic Technol.*, *22*(1), 3–17.

Cochran, D. R., and R. L. Pyle (1978), Volcanology via satellite, Mon, *Weather Rev.*, *106*, 1373–1375.

Derber, J. C., D. F. Parrish, and S. J. Lord (1991), The new global operational analysis system at the National Meteorological Center, *Weather Forecasting*, *6*, 538–547.

Duggen, S., P. Croot, U. Schacht, and L. Hoffmann (2007), Subduction zone volcanic ash can fertilize the surface ocean and stimulate phytoplankton growth: Evidence from biogeochemical experiments and satellite data, *Geophys. Res. Lett.*, *34*, L01612, doi:10.1029/2006GL027522.

Eckermann, S. D., D. Broutman, J. Ma, and J. Lindeman (2006), Fourier-ray modeling of short-wavelength trapped lee waves observed in infrared satellite imagery near Jan Mayen, *Mon. Weather Rev.*, *134*(10), 2830–2848.

Ferek, R. J., D. A. Hegg, P. V. Hobbs, P. Durkee, and K. Nielsen (1998), Measurements of ship-induced tracks in clouds off the Washington coast, *J. Geophys. Res.*, *103*(D18), 23,199–23,206.

Gavati, A., and D. Rosenfeld (2004), Quantifying precipitation suppression due to air pollution, *J. Appl. Meteorol.*, *43*, 1038–1056.

Graf, H. F., J. Feichter, and B. Langmann (1997), Volcanic sulfur emissions: Estimates of source strength and its contribution to the global sulfate distribution, *J. Geophys. Res.*, *102*(D9), 10,727–10,738.

Graf, H.-F., B. Langmann, and J. Feichter (1998), The contribution of Earth degassing to the atmospheric sulfur budget, *Chem. Geol.*, *147*, 131–145.

Guo, H., J. E. Penner, M. Herzog, and H. Pawlowska (2006), Examining aerosol indirect effect under contrasting environments during the ACE-2 experiment, *Atmos. Chem. Phys. Disc.*, *6*, 11,561–11,596.

Halmer, M. M., H.-U. Schmincke, and H.-F. Graf (2002), The annual volcanic gas input into the atmosphere, in particular into the stratosphere: A global data set for the past 100 years, *J. Volcanol. Geotherm. Res.*, *115*(3–4), 511–528.

Hegg, D. A., K. Nielsen, D. S. Covert, H. H. Jonsson, and P. A. Durkee (2007), Factors influencing the mesoscale variations in marine stratocumulus albedos, *Tellus, Ser. B*, *59*(1), 66–76, doi:10.1111/j.1600-0889.2006.00231.x.

Heiken, G. (1994), Volcanic ash: What it is and how it forms, in *Volcanic Ash and Aviation Safety—Proceedings of the First International Symposium on Volcanic Ash and Aviation Safety*, edited by T. J. Casadevall, *U.S. Geol. Surv. Bull.*, *2047*, 39–45.

Hobbs, P., and A. Rangno (1998), Microstructures of low and middle-level clouds over the Beaufort Sea, *Q. J. R. Meteorol. Soc.*, *124*, 2035–2071.

Holdgate, M. W., and P. E. Baker (1979), The South Sandwich Islands, general description, *Br. Antarct. Surv. Sci. Rep.*, *91*, 76 pp.

Horváth, Á., and R. Davies (2007), Comparison of microwave and optical liquid water path estimates from TMI, MODIS, and MISR, *J. Geophys. Res.*, *112*, D01202, doi:10.1029/2006JD007101.

Intergovernmental Panel on Climate Change (2001), *Climate Change 2001: The Scientific Basis—Contribution of Working Group I to the Third Assessment Report of the Intergovernmental Panel on Climate Change*, edited by J. T. Houghton et al., 881 pp., Cambridge Univ. Press, New York.

Kaufman, Y. J., and R. S. Fraser (1997), The effect of smoke particles on clouds and climate forcing, *Science*, *277*, 1636–1639.

Kaufman, Y. J., and T. Nakajima (1993), Effect of Amazon smoke on cloud microphysics and albedo—Analysis from satellite imagery, *J. Appl. Meteorol.*, *32*, 729–744.

King, M. D., Y. J. Kaufman, W. P. Menzel, and D. Tanré (1992), Remote sensing of cloud, aerosol, and water vapor properties from the Moderate Resolution Imaging Spectrometer (MODIS), *IEEE Trans. Geosci. Remote Sens.*, *30*, 2–27.

King, M. D., W. P. Menzel, Y. J. Kaufman, D. Tanré, B. C. Gao, S. Platnick, S. A. Ackerman, L. A. Remer, R. Pincus, and P. A. Hubanks (2003), Cloud and aerosol properties, precipitable water, and profiles of temperature and humidity from MODIS, *IEEE Trans. Geosci. Remote Sens.*, *41*, 442–458.

Kinoshita, K. (1996), Observation of flow and dispersion of volcanic clouds from Mt. Sakurajima, *Atmos. Environ.*, *30*(16), 2831–2837.

Kinoshita, K., C. Kanagaki, N. Iino, M. Koyamada, A. Terada, and A. Tupper (2003), Volcanic plumes at Miyakejima observed from satellites and from the ground, *Proc. SPIE Int. Soc. Opt. Eng.*, *4891*, 227–236.

Krotkov, N. A., S. A. Carn, A. J. Krueger, P. K. Bhartia, and K. Yang (2006), Band residual difference algorithm for retrieval of SO_2 from the Aura Ozone Monitoring Instrument (OMI), *IEEE Trans. Geosci. Remote Sens.*, *44*(5), 1259–1266.

Lachlan-Cope, T., J. L. Smellie, and R. Ladkin (2001), Discovery of a recurrent lava lake on Saunders Island (South Sandwich Islands) using AVHRR imagery, *J. Volcanol. Geotherm. Res.*, *112*, 105–116.

Lin, J. C., T. Matsui, R. A. Pielke Sr., and C. Kummerow (2006), Effects of biomass burning-derived aerosols on precipitation and clouds in the Amazon Basin: A satellite-based empirical study, *J. Geophys. Res.*, *111*, D19204, doi:10.1029/2005JD006884.

Marshak, A., S. Platnick, T. Varnai, G. Wen, and R. F. Cahalan (2006), Impact of 3D radiative effects on satellite retrievals of cloud droplet sizes, *J. Geophys. Res.*, *111*, D09207, doi:10.1029/2005JD006686.

Masunaga, H., S. M. Kreidenweis, R. A. Pielke Sr., W.-K. Tao, M. Chin, and Y. J. Kaufman (2006), Satellite-based assessment of marine low cloud variability associated with aerosol, atmospheric stability, and the diurnal cycle, *J. Geophys. Res.*, *111*, D17204, doi:10.1029/2005JD006097.

Mather, T. A., D. M. Pyle, and C. Oppenheimer (2003), Tropospheric volcanic aerosol, in *Volcanism and the Earth's Atmosphere*, *Geophys. Monogr. Ser.*, vol. 139, edited by A. Robock and C. Oppenheimer, pp. 189–212, AGU, Washington, D. C.

Mather, T. A., C. Oppenheimer, A. G. Allen, and A. J. S. McGonigle (2004), Aerosol chemistry of emissions from three contrasting volcanoes in Italy, *Atmos. Environ.*, *38*(33), 5637–5649.

Matsushima, N., and H. Shinohara (2006), Visible and invisible volcanic plumes, *Geophys. Res. Lett.*, *33*, L24309, doi:10.1029/2006GL026506.

Meskhidze, N., W. Chameides, A. Nenes, and G. Chen (2003), Iron mobilization in mineral dust: Can anthropogenic SO_2 emissions affect ocean productivity?, *Geophys. Res. Lett.*, *30*(21), 2085, doi:10.1029/2003GL018035.

Miles, N. L., J. Verlinde, and E. E. Clothiaux (2000), Cloud droplet size distributions in low-level stratiform clouds, *J. Atmos. Sci.*, *57*, 295–311.

Naud, C. M., J. P. Muller, E. E. Clothiaux, B. A. Baum, and W. P. Menzel (2005), Intercomparison of multiple years of MODIS, MISR and radar cloud-top heights, *Ann. Geophys.*, *23*(7), 2415–2424.

Patrick, M., J. L. Smellie, A. J. L. Harris, R. Wright, K. Dean, P. Izbekov, H. Garbeil, and E. Pilger (2005), First recorded eruption of Mount Belinda volcano (Montagu Island), South Sandwich Islands, *Bull. Volcanol.*, *67*, 415–422.

Platnick, S., P. A. Durkee, K. Nielson, J. P. Taylor, S. C. Tsay, M. D. King, R. J. Ferek, P. V. Hobbs, and J. W. Rottman (2000), The role of background cloud microphysics in the radiative formation of ship tracks, *J. Atmos. Sci.*, *57*, 2607–2624.

Platnick, S., M. D. King, S. A. Ackerman, W. P. Menzel, B. A. Baum, J. C. Riedi, and R. A. Frey (2003), The MODIS cloud products: Algorithms and examples from Terra, *IEEE Trans. Geosci. Remote Sens.*, *41*(2), 459–473.

Prata, F. (1989), Observations of volcanic ash clouds in the 10–12 μm window using AVHRR/2 data, *Int. J. Remote Sens.*, *10*, 751–761.

Radke, L. F., J. A. Coakley Jr., and M. D. King (1989), Direct and remote sensing observations of the effects of ships on clouds, *Science*, *246*, 1146–1149.

Ramanathan, V., et al. (2001a), Indian Ocean Experiment: An integrated analysis of the climate forcing and effects of the great Indo-Asian haze, *J. Geophys. Res.*, *106*(D22), 28,371–28,398.

Ramanathan, V., P. J. Crutzen, J. T. Kiehl, and D. Rosenfeld (2001b), Atmosphere—Aerosols, climate, and the hydrological cycle, *Science*, *294*(5549), 2119–2124.

Robock, A. (2000), Volcanic eruptions and climate, *Rev. Geophys.*, *38*, 191–220.

Rose, W. I., G. Heiken, K. Wohletz, D. Eppler, S. Barr, T. Miller, R. L. Chuan, and R. B. Symonds (1988), Direct rate measurements of eruption plumes at Augustine Volcano: A problem of scaling and uncontrolled variables, *J. Geophys. Res.*, *93*, 4485–4499.

Rosenfeld, D. (1999), TRMM observed first direct evidence of smoke from forest fires inhibiting rainfall, *Geophys. Res. Lett.*, *26*(20), 3105–3108.

Rosenfeld, D. (2000), Suppression of rain and snow by urban air pollution, *Science*, *287*, 1793–1796.

Rosenfeld, D., Y. J. Kaufman, and I. Koren (2006), Switching cloud cover and dynamical regimes from open to closed Benard cells in response to the suppression of precipitation by aerosols, *Atmos. Chem. Phys. Disc.*, *6*, 1179–1198.

Rudich, Y., A. Sagi, and D. Rosenfeld (2003), Influence of the Kuwait oil fires plume [1991] on the microphysical development of clouds, *J. Geophys. Res.*, *108*(D15), 4478, doi:10.1029/2003JD003472.

Russell, P. B., et al. (1993), Pinatubo and pre-Pinatubo optical-depth spectra: Mauna Loa measurements, comparisons, inferred particle size distributions, radiative effects, and relationship to lidar data, *J. Geophys. Res.*, *98*(D12), 22,969–22,985.

Sarmiento, J. L. (1993), Atmospheric CO_2 stalled, *Nature*, *365*, 697–698, doi:10.1038/365697a0.

Schreier, M., A. A. Kokhanovsky, V. Eyring, L. Bugliaro, H. Mannstein, B. Mayer, H. Bovensmann, and J. P. Burrows (2006), Impact of ship emissions on the microphysical, optical and radiative properties of marine stratus: A case study, *Atmos. Chem. Phys. Disc.*, *6*, 1023–1071.

Segrin, M. S., J. A. Coakley Jr., and W. R. Tahnk (2007), MODIS observations of ship tracks in summertime stratus off the west coast of the U.S., *J. Atmos. Sci.*, *64*(12), 4330–4345.

Self, S., and G. P. L. Walker (1994), Ash clouds: Characteristics of eruption columns, in *Volcanic Ash and Aviation Safety: Proceedings of the First International Symposium on Volcanic Ash and Aviation Safety,* edited by T. J. Casadevall, *U.S. Geol. Surv. Bull.*, *2047*, 65–74.

Sharman, R. D., and M. G. Wurtele (1983), Ship waves and lee waves, *J. Atmos. Sci.*, *40*, 396–427.

Siebert, L., and T. Simkin (2002), *Volcanoes of the World: An Illustrated Catalog of Holocene Volcanoes and Their Eruptions, Global Volcanism Program Digital Inf. Ser., GVP-3*, Smithsonian Inst., Washington, D. C. (Available at http://www.volcano.si.edu/world/)

Simkin, T. (1994), Volcanoes—Their occurrence and geography, in *Volcanic Ash and Aviation Safety: Proceedings of the First International Symposium on Volcanic Ash and Aviation Safety*, edited by T. J. Casadevall, *U.S. Geol. Surv. Bull.*, *2047*, 75–80.

Sinclair, M. R. (1994), An objective cyclone climatology for the Southern Hemisphere, *Mon. Weather Rev.*, *122*, 2239–2256.

Smithsonian Institution, (2005), Montagu Island, *Bull. Global Volcanism Network*, *30*(9).

Smithsonian Institution (2006), Montagu Island, *Bull. Global Volcanism Network*, *31*(3).

Stephens, G. L. (1978), Radiation profiles in extended water clouds. II: Parameterization schemes, *J. Atmos. Sci.*, *35*, 2123–2132.

Stevens, B., et al. (2003), Dynamics and Chemistry of Marine Stratocumulus-DYCOMS-II, *Bull. Am. Meteorol. Soc.*, *84*, 579–593.

Stevens, B., G. Vali, K. Comstock, R. Wood, M. C. Zanten, P. Austin, C. S. Bretherton, and D. H. Lenschow (2005), Pockets of open cells (POCs) and drizzle in marine stratocumulus, *Bull. Am. Meteorol. Soc.*, *86*, 51–57.

Stoiber, R. E., S. N. Williams, and B. Huebert (1987), Annual contribution of sulfur dioxide to the atmosphere by volcanoes, *J. Volcanol. Geotherm. Res.*, *33*, 1–8.

Tupper, A., J. S. Oswalt, and D. Rosenfeld (2005), Satellite and radar analysis of the volcanic-cumulonimbi at Mt Pinatubo, Philippines, 1991, *J. Geophys. Res.*, *110*, D09204, doi:10.1029/2004JD005499.

Twohy, C. H., M. D. Petters, J. R. Snider, B. Stevens, W. Tahnk, M. Wetzel, L. Russell, and F. Burnet (2005), Evaluation of the aerosol indirect effect in marine stratocumulus clouds: Droplet number, size, liquid water path, and radiative impact, *J. Geophys. Res.*, *110*, D08203, doi:10.1029/2004JD005116.

Twomey, S. (1991), Aerosols, clouds and radiation, *Atmos. Environ.*, *25A*(11), 2435–2442.

Uematsu, M., M. Toratani, M. Kajino, Y. Narita, Y. Senga, and T. Kimoto (2004), Enhancement of primary productivity in the western North Pacific caused by the eruption of the Miyake-jima Volcano, *Geophys. Res. Lett.*, *31*, L06106, doi:10.1029/2003GL018790.

Vant-Hull, B., A. Marshak, L. Remer, and Z. Li (2007), The effects of scattering angle and cumulus cloud geometry on satellite retrievals of cloud drop effective radius, *Geosci. Remote Sens. Lett.*, *45*(4), 1039–1045.

Varnai, T., and A. Marshak (2007), View angle dependence of cloud optical thickness retrieved by MODIS, *J. Geophys. Res.*, *112*, D06203, doi:10.1029/2005JD006912.

Watson, A. J. (1997), Volcanic iron CO_2, ocean productivity and climate, *Nature*, *385*, 587–588, doi:10.1038/385587b0.

Wentz, F. (1997), A well-calibrated ocean algorithm for Special Sensor Microwave/Imager, *J. Geophys. Res.*, *102*, 8703–8718.

Wentz, F., and T. Meissner (2000), AMSR ocean algorithm, *Algorithm Theor. Basis Doc. 121599A-1*, Remote Sens. Syst., Santa Rosa, Calif. (Available at http://www.ssmi.com/support/publications.html)

Wright, R., L. P. Flynn, H. Garbeil, A. J. L. Harris, and E. Pilger (2004), MODVOLC: Near-real-time thermal monitoring of global volcanism, *J. Volcanol. Geotherm. Res.*, *135*, 29–49.

Wood, R., C. S. Bretherton, and D. L. Hartmann (2002), Diurnal cycle of liquid water path over the subtropical and tropical oceans, *Geophys. Res. Lett.*, *29*(23), 2092, doi:10.1029/2002GL015371.

S. Gassó, NASA Goddard Space Flight Center, Code 613.2, Greenbelt, MD 20771, USA. (santiago@climate.gsfc.nasa.gov)